IMAGE RESTORATION USING CONTENT-ADAPTIVE MESH MODELING[1]

Jovan G. Brankov, Yongyi Yang, and Nikolas P. Galatsanos

Dept. of Electrical and Computer Engineering
Illinois Institute of Technology
3301 S. Dearborn St., Chicago, IL 60616, USA

ABSTRACT

In this work we explore the use of a content-adaptive mesh model (CAMM) in the classical problem of image restoration. In the proposed framework, we first model the image to be restored by an efficient mesh representation. A CAMM can be viewed as a form of image representation using non-uniform samples, of which the mesh nodes (i.e., image samples) are adaptively placed according to the local content of the image. The image is then restored through estimating the model parameters (i.e., mesh nodal values) from the data. A CAMM provides a natural spatially-adaptive regularization mechanism for image restoration in that the interpolation basis functions in a CAMM have their spatial support varying with the local image content. We present some exploratory results to demonstrate the proposed approach.

1. INTRODUCTION

Mesh modeling of an image involves partitioning the image domain into a collection of non-overlapping (generally polygonal) patches called *mesh elements*. The image function is then determined over each element by interpolation based on the values at the vertices, called *mesh nodes*, of the element. Mesh modeling has recently found many important applications in image processing, including image compression, motion tracking and compensation, image processing through geometric manipulation, and medical image analysis (e.g., [1-7]).

In our previous work we developed a fast and accurate approach for image representation using a content-adaptive mesh model (CAMM) [8], and applied this approach to tomographic image reconstruction [9,10]. The CAMM is essentially a form of image representation based on non-uniform sampling. Specifically, in a CAMM smaller mesh elements (hence more samples) are placed in regions of an image containing high frequency features, while larger elements are placed in regions containing predominantly low frequency components.

In this paper we extend our previous work by exploring the use of a CAMM in the classical problem of image restoration. In this approach we first represent the image to be restored by a CAMM, and then determine the image by estimating the values of the mesh nodes from the observed data. Our goal is to establish a basic framework for the proposed mesh-modeling approach for image restoration, and to investigate the feasibility and benefits of this approach.

The use of a CAMM for image restoration may have several potential benefits. First, a CAMM is a compact image representation, i.e., an image can be represented using far fewer mesh nodes than pixels. Thus, a CAMM improves efficiency of restoration algorithms, and can help alleviate the underdetermined nature of the reconstruction problem. Second, a CAMM provides a natural spatially-adaptive smoothness mechanism. Finally, a CAMM serves as a natural framework for restoration of moving image sequences, wherein mesh elements are allowed to deform over time.

In the literature a great many methods have been developed for improving the quality of restored images (see [11] for a review). All of these methods are pixel-based, i.e., the image is represented and computed directly in a pixel basis. These methods achieve their aim by introducing *a priori* information about the image being restored to combat the effect of noise in the imaging data. For example, in a classical Bayesian approach a prior probability model is assumed on the image, then the solution is found according to the maximum *a posterior* (MAP) criterion (e.g., [12-14]). With a similar goal to the Bayesian methods, deterministic regularization methods (e.g., [15-18]) have also been studied. In this paper we propose the use of mesh modeling as an alternative approach to achieve spatially adaptive regularization.

2. PROBLEM FORMULATION

2.1 Mesh representation

Let $f(\mathbf{x})$ denote an image function defined over a domain D. In a mesh model the domain D is partitioned into M non-overlapping mesh elements, denoted by D_m, $m=1,2,\cdots,M$, so that $D=\bigcup_{m=1}^{M} D_m$ (see Fig. 1(c)). The function $f(\mathbf{x})$ is then represented by interpolation over each element D_m from the values of its nodes.

For convenience we denote the mesh nodes using a single index as $\mathbf{x}_n$, $n=1,2,\ldots,N$, with the understanding that any given mesh node is typically shared among

[1] This research was supported in part by the Whitaker Foundation.

0-7803-7750-8/03/$17.00 ©2003 IEEE

several elements. The mesh representation for $f(\mathbf{x})$ can be written in the image domain D as follows:

$$f(\mathbf{x})=\sum_{n=1}^{N} f(\mathbf{x}_n)\phi_n(\mathbf{x})+e(\mathbf{x}), \tag{1}$$

where $\phi_n(\mathbf{x})$ is the interpolation function associated with node n, and $e(\mathbf{x})$ is the interpolation error. The support of $\phi_n(\mathbf{x})$ is strictly limited to these elements attached to node n.

It is apparent that the mesh representation in (1) is an image description based on non-uniform sampling, wherein the mesh nodes are the sample points. In our previous work [8] we proposed a fast algorithm that can strategically place the mesh elements (and thus the nodes) according to the local content of the image, with samples placed most densely in areas having the most image detail. Herein we use this method as part of a new approach to image restoration.

2.2 Image restoration using a mesh model

Our goal is to use a mesh model as a basis for estimation of $f(\mathbf{x})$ from the noisy data $g(\mathbf{x})$. In image restoration, the observed noisy data can be modeled by

$$g(\mathbf{x})=\int_D f(\mathbf{y})h(\mathbf{y}-\mathbf{x})dy+n(\mathbf{x}), \tag{2}$$

where $h(\mathbf{x})$ denotes the point spread function (PSF) of the imaging system, and $n(\mathbf{x})$ is the additive noise.

Substituting (1) into (2) we obtain:

$$g(\mathbf{x})=\sum_{n=1}^{N}\left[f(\mathbf{x}_n)\int_D \phi_n(\mathbf{y})h(\mathbf{y}-\mathbf{x})dy\right] + \int_D e(\mathbf{y})h(\mathbf{y}-\mathbf{x})dy+n(\mathbf{x}). \tag{3}$$

Defining

$$a_n(\mathbf{x})=\int_D \phi_n(\mathbf{y})h(\mathbf{y}-\mathbf{x})dy \tag{4}$$

and

$$\hat{e}(\mathbf{x})=\int_D e(\mathbf{y})h(\mathbf{y}-\mathbf{x})dy, \tag{5}$$

we rewrite (3) as

$$g(\mathbf{x})=\sum_{n=1}^{N} f(\mathbf{x}_n)a_n(\mathbf{x})+\hat{e}(\mathbf{x})+n(\mathbf{x}). \tag{6}$$

A few remarks are in order. First, it is evident from (4) that the term $a_n(\mathbf{x})$ represents the noise-free response by the PSF to an impulse placed at the nth node in the mesh model. Second, from (5) it is clear that $\hat{e}(\mathbf{x})$ is simply the mesh modeling error blurred by the PSF. As demonstrated in our previous work [8], a CAMM can provide a very accurate image representation; therefore the interpolation error $\hat{e}(\mathbf{x})$ is often negligible compared to the imaging noise. Thus, the noise statistics in (6) is dominated by that of $n(\mathbf{x})$.

Let $\mathbf{g}$ denote a vector formed by a lexicographic ordering of the pixel values representing the data $g(\mathbf{x})$; similarly, let $\mathbf{a}_n$ represent the response $a_n(\mathbf{x})$, and $\mathbf{n}$ represent the total noise $\hat{e}(\mathbf{x})+n(\mathbf{x})$ in (6). Moreover, let the matrix $\mathbf{A}\equiv[\mathbf{a}_1,\mathbf{a}_1,\cdots,\mathbf{a}_N]$, formed by all the vectors $\mathbf{a}_n$. Then, from (6) we obtain the mesh-domain model

$$\mathbf{g}=\mathbf{A}\mathbf{f}_m+\mathbf{n}. \tag{7}$$

where $\mathbf{f}_m\equiv[f(\mathbf{x}_1),f(\mathbf{x}_2),\cdots,f(\mathbf{x}_N)]^T$, i.e., a vector formed from the nodal values of the mesh model.

Based on (7) the restoration problem becomes that of estimating $\mathbf{f}_m$ from the observed data $\mathbf{g}$ through the system matrix $\mathbf{A}$. The image $\mathbf{f}$ can then be obtained by using (1) (neglecting $e(\mathbf{x})$). Implementation issues related to $\mathbf{A}$ are discussed in Section 3.

2.3 Restoration algorithms

The mesh-domain imaging model (7) has precisely the same form as the conventional pixel-domain imaging model. In this study we consider both maximum-likelihood (ML) and maximum *a posteriori* (MAP) methods.

Maximum-likelihood solution

ML estimation is based on solution of the following problem

$$\hat{\mathbf{f}}_m=\arg\max_{\mathbf{f}_m}\left[\log p(\mathbf{g};\mathbf{f}_m)\right], \tag{8}$$

where $p(\mathbf{g};\mathbf{f}_m)$ is the likelihood function of $\mathbf{g}$ parameterized by $\mathbf{f}_m$.

In this paper, we assume an additive white Gaussian noise model. The ML estimate in (8) is then determined by minimizing a weighted squared error, i.e.,

$$\hat{\mathbf{f}}_m=\arg\min_{\mathbf{f}_m}\left\|\mathbf{W}(\mathbf{g}-\mathbf{A}\mathbf{f}_m)\right\|^2, \tag{9}$$

where $\|\cdot\|$ is the Euclidean norm, and $\mathbf{W}$ is a weighting matrix defined according to the noise level in the data $\mathbf{g}$.

Maximum *a posteriori* (MAP) solution

Assume $p(\mathbf{f}_m)$ a prior on the unknown nodal values $\mathbf{f}_m$. Then the MAP estimate is obtained as:

$$\hat{\mathbf{f}}_m=\arg\max_{\mathbf{f}_m}\left[\log p(\mathbf{g};\mathbf{f}_m)+\log p(\mathbf{f}_m)\right]. \tag{10}$$

In this study we assume a Gibbs prior $p(\mathbf{f}_m)$, i.e.,

$$p(\mathbf{f}_m)\sim\exp\left[-\beta U(\mathbf{f}_m)\right], \tag{11}$$

where β is a scalar weighting parameter, and the potential function $U(\mathbf{f}_m)$ is defined as:

$$U(\mathbf{f}_m)=\sum_{n=1}^{N}\sum_{j\in\Re_n}\left[f(\mathbf{x}_j)-f(\mathbf{x}_n)\right]^2, \tag{12}$$

where $\Re_n$ denotes the index set of nodes connected to node n.

Under the assumption of an additive white Gaussian noise model, the MAP estimate in (11) can then be computed by solving the following optimization problem:

$$\hat{\mathbf{f}}_m = \arg\min_{\mathbf{f}_m}\left\{\left\|\mathbf{W}(\mathbf{g}-\mathbf{A}\mathbf{f}_m)\right\|^2 + \beta\sum_{n=1}^{N}\sum_{j\in\Re_n}\left[f(\mathbf{x}_j)-f(\mathbf{x}_n)\right]^2\right\} \quad (13)$$

The solution in (13) has a form similar to that of regularized least-squares in the pixel domain [15]. The objective function in (3) is of a quadratic form. In this study we used the conjugate gradient algorithm to perform the optimization.

3. IMPLEMENTATION ISSUES

3.1. Content-adaptive mesh generation

In [8] we developed a fast, non-iterative approach, based on a simple half-toning procedure, that can produce a very accurate mesh representation for a given image $f(\mathbf{x})$. Of course, here the image $f(\mathbf{x})$ to be restored is not known beforehand. Instead, we substitute $f(\mathbf{x})$ with a *reference image* $\tilde{f}(\mathbf{x})$, the purpose of which is to provide an estimate of the distribution of the local image content, according to which the mesh nodes are then placed. A reference image can be obtained from a preliminary restoration of the image using a simple algorithm, or even from simple low pass filtering of the noisy image.

3.2. Computation of mesh-domain system matrix

Once the mesh is obtained, the mesh-domain system matrix $\mathbf{A}$ is then computed according to (4). This task can be greatly simplified by taking advantage of the fact that $\phi_n(\mathbf{x})$ has only limited support and that the integration in (4) can be calculated through the use of a so-called *master element* [4], a technique developed in the field of finite-element analysis. A particularly appealing case is when the analytical form of the PSF $h(\mathbf{x})$ is known; the integration in (4) can then be pre-calculated in an analytical form. In this study, we simply measured $\mathbf{A}$ by probing the input with an impulse function.

4. EXPERIMENTAL RESULTS

4.1 Mesh filtering of noisy images

In this section we present some results to demonstrate that the proposed mesh representation provides a natural spatially-adaptive regularization scheme. For better visualization of the results, a 128×128 section cropped from the original 256×256 image "Lena" was used as a test image (Fig. 1.(a)). Shown in Fig. 1.(b) is this image corrupted with additive white Gaussian noise (PSNR=25.91 dB). For mesh generation this noisy image was first processed by lowpass filtering (bandwidth=0.8π rad/pixel), followed by the mesh generation procedure in [8]. The resulting mesh structure is shown in Fig. 1(c), in which N=4,042 mesh nodes were used. Next, this mesh was applied to restore the image according to the ML estimate in (9). Here $\mathbf{A}$ is simply the matrix $\mathbf{\Phi}$ since no blurring was used; $\mathbf{W}$ was chosen as the identity matrix (for stationary white noise). The restored image is shown in Fig. 1.(d), PSNR=28.69 dB. Similar results were obtained when different number of mesh nodes was used.

For comparison, we show in Figs. 1.(e) and (f) images obtained using adaptive Wiener filtering [19] and median filtering of the noisy image, respectively. Note that most of the high-frequency features (such as edges and textures) are better preserved in the mesh restored image in Fig. 1.(d).

4.2. Mesh de-blurring

Shown in Fig. 2(a) is the Lena image first blurred by a 2D Gaussian kernel (std=2 pixels), followed by addition of white Gaussian noise at a level of SNR=29.90 dB. The image was then lowpass filtered (bandwidth=0.8π rad/pixel) to produce a reference image for mesh generation. The resulting mesh structure, having 6,500 mesh nodes, was then used to restore the image according to the MAP estimate in (13); the obtained image is shown in Fig. 2(b), PSNR=28.77 dB. In (13) $\beta = 0.05$ was used.

For comparison purpose, we show in Fig. 2(c) an image obtained with a Wiener inverse filter, where the signal spectrum was estimated from the image data. In Fig. 2(d) we show an image obtained using a pixel based regularized restoration [15]. Here the Laplacian operator was used in the regularization term and the regularization parameter was selected using a trial-and-error process to find the optimal value.

Similar results were also obtained at different degrees of blurring and noise level. These results are not shown here, but will be presented at the conference.

5. CONCLUSIONS

In this paper we proposed a mesh modeling approach for image restoration. A key feature in this mesh model is that it is customized for the image, having an essential form of non-uniform sampling where samples are placed most densely in areas that contain significant detail. Our preliminary results demonstrate that the proposed approach can yield good results for image restoration, at least competitive to that of pixel-based approaches.

6. REFERENCES

[1] K. Aizawa and T. S. Huang, *Proc. IEEE*, vol. 83, pp. 259-271, Feb. 1995.

[2] F. Davoine, M. Antonini, J. Chassery, and M. Barlaud, *IEEE Trans. Image Proc.*, vol. 5, pp. 338-346, 1996.

[3] L. Demaret, G. Robert, N. Laurent, A. Buisson, *Proc. IEEE Intl. Conf. Image Processing*, vol.3, pp.849-852, Vancouver, 2000.

[4] Y. Wang and O. Lee, *IEEE Trans. Image Processing*, vol. 3, no. 5, pp. 610-624, 1994.

[5] Y. Altunbasak and A. M. Tekalp, *IEEE Trans. Image Processing*, vol. 6, no. 9, pp. 1255-1269, 1997.

[6] M. A. Garcia and B. X. Vintimilla, *Proc. IEEE Intl. Conf. Image Processing*, vol. 1, pp. 97-100, Vancouver, Sept., 2000.

[7] A. Singh, *et al*, ed., *Deformable Models in Medical Image Analysis*, IEEE Computer Society Press, 1998.

[8] Y. Yang, J. Brankov, and M. N. Wernick, *Proc. IEEE Intl. Conf. Image Processing*, vol. 1, pp. 868-871, Greece, Oct., 2001.

[9] J. G. Brankov, Y. Yang, M. V. Narayanan, and M. N. Wernick, presented at *Fully 3D Image Recon. In Radiol. and Nucl. Med.*, Pacific Grove, California, USA, 2001.

[10] Y. Yang, J. G. Brankov, and M. N. Wernick, *Proc. IEEE Intl. Conf. Image Processing*,, vol. 2, pp. 621-624, Rochester, New York, Sept. 22-25, 2002.

[11] M. R. Banham, A. K. Katsaggelos, *IEEE Signal Processing Mag.*, vol. 14, no. 2, pp. 24-41, 1997.

[12] S. Geman and D. Geman, *IEEE Trans. Pattern Anal. and Machine Intell.*, vol. 6, pp. 228-238, 1984.

[13] C. Bouman and K. Sauer, *IEEE Trans. Image Processing*, vol. 2, pp. 296-310, 1993.

[14] T. J. Hebert and K. Lu, *IEEE Trans. Image Processing*, vol. 4, no. 8, pp.1084-1095, 1995.

[15] N. P. Galatsanos and A. K. Katsaggelos, *IEEE Trans. Image Processing*, vol. 1, no. 3, pp. 322-336, 1992.

[16] J. Biemond, A. K. Katsaggelos, R. M. Mersereau, R. W. Schafer, *IEEE Trans. Signal Processing*, vol. 39, no. 4, pp. 914-929, 1991.

[17] F. C. Jeng and J. W. Woods, *IEEE Trans. Signal Processing*, vol.39, no.3, pp.683-697, 1991.

[18] P. Charbonnier, L. Blanc-Féraud, G. Aubert, M. Barlaud, *IEEE Trans. Image Processing*, vol.6, no.2, pp.298-311, 1997.

[19] J. S. Lim, *Two-Dimensional Signal and Image Processing*, Prentice-Hall, Inc., pp.536-540, 1990.

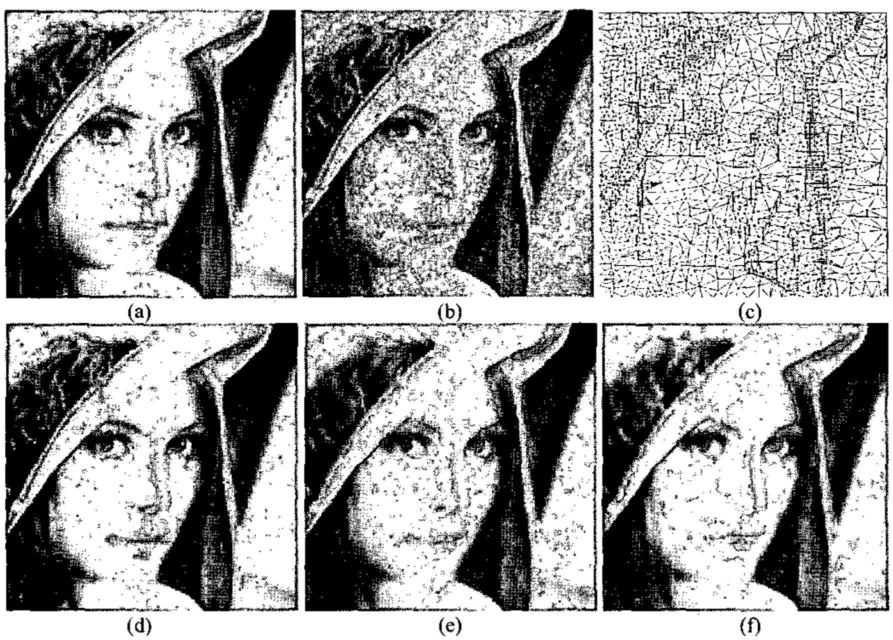

Figure 1. (a) A 128×128 section of the original Lena image; (b) the image in (a) corrupted with additive white Gaussian noise, PSNR=25.91 dB; (c) mesh structure generated from the noisy image in (b) after lowpass filtering, N=4,042 mesh nodes used; (d) image restored from ML estimation with the mesh in (c), PSNR=28.69dB; (e) image obtained using Wiener filtering, PSNR= 29.14dB; (f) image obtained using median filtering, PSNR= 27.61dB. Note that most of the high-frequency features (such as edges and textures) are better preserved in the mesh-restored image in (d), even though the image from adaptive Wiener filtering has a slightly higher PSNR.

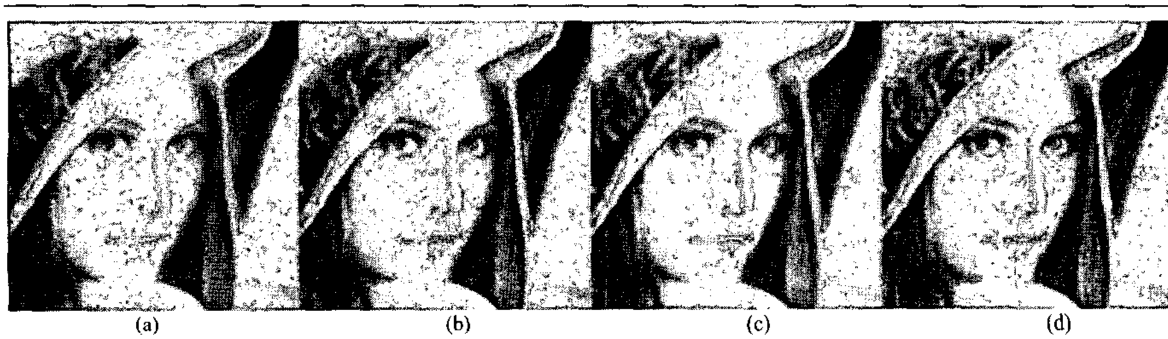

Figure 2. (a) Lena image degraded with a Gaussian blur and additive noise; (b) image restored with mesh based approach, PSNR=28.77 dB; (c) image restored using Wiener inverse filter, PSNR=28.15dB; and (d) image obtained using pixel based restoration, PSNR=28.52 dB.